AN ENERGY-BASED SEGMENTATION OF PROSTATE FROM ULTRASOUIND IMAGES USING DOT-PATTERN SELECT CELLS

Amjad Zaim[1] *and Jerzy Jankun*[2]
[1]Computer Science Department, University of Texas at Brownsville,
Brownsville, Texas, USA 78520
[2]Urology Research Center, Department of Urology, Medical University of Ohio,
Toledo, OH 43699-0008, USA
[1]amjad.zaim@utb.com, [2]jjankun@meduohio.edu

ABSTRACT

Automatic segmentation of prostate boundaries from Transrectal Ultrasound (TRUS) images still poses significant challenge in minimally-invasive surgical procedures. The presence of strong speckle noise and shadow artifacts limits the effectiveness of classical segmentation schemes. Several model-based and feature-approaches have been proposed for segmentation of the prostate. In this paper, we propose a new energy-based method for segmentation of ultrasound prostate images using active contour modeling guided by dot-pattern textural energy map. First, impulsive noise and speckles are reduced with median filtering and top-hat transform. Prostate features are then extracted from the filtered images using non-linear dot-pattern select operator. An elastic template shape model that incorporates a priori knowledge of the average geometric shape of the prostate boundaries as well as the energy derived from the dot-pattern feature image are utilized to search for the optimal prostate contour. A number of experiments comparing the extracted contours with manually-delineated contours validated the performance of our method.

Index Terms— Prostate, Segmentation, Transrectal Ultrasound, Dot-Pattern Select Cells, Active Contour

1. INTRODUCTION

Prostate cancer remains the most commonly diagnosed cancer in men and the second highest North American mortality rate among all cancers in men, surpassed only by lung cancer [1]. Modern diagnosis and treatment methods, such as needle-biopsy and brachytherapy respectively, takes into account the 2D geometric distribution of the prostate as imaged by ultrasound to map out an effective and accurate treatment plan. The relatively inexpensive and safe use of ultrasound makes it an attractive imaging modality compared to other imaging tools such as MRI and CT. To image the prostate, a cylinder shape probe, also called transrectal probe, is inserted into the rectum and rotated to scan the entire prostate capsule. The produced scans are ultimately used to reconstruct a 3-D model of the prostate [1,2]. In addition, the safety associated with ultrasound allows for real time monitoring of the prostate gland and accounts for any anatomical displacement. However, the main drawback of ultrasound stems from the presence of speckles and artifacts arising from constructive-destructive interference of the reflected waves. Ultrasound prostate images are highly corrupted with noise which prevents accurate localization of the gland. As a result, most modern treatment planning tools rely on manual outlining of the prostate; a tedious process that requires extensive labor time and comes at the expense of spatial resolution particularly when large number of 2D images are available. While many research studies have had some success in segmenting the prostate boundaries from ultrasound images with minimal human intervention, only limited progress has been reported. Researchers designed a 3D discrete active deformable model to outline the prostate using initial polygonal contours defined in a number of slices and using edge maps to drive the deformation model [3,4]. Others have developed an algorithm for detecting prostate edges as a visual guidance for the user to manually follow [5]. Statistical shape models have also been applied to segment and differentiate between the various shapes of prostates using prior knowledge of the prostate region in ultrasound images. Neural Network has also been utilized to recognize the prostate geometry from a database of prostate shapes. Gabor filtering was designed to extract prostate features and train a KSVM neural network [6]. Adaptive edge-detection methods were also employed [7]. Despite that some of these studies have reported accurate segmentation results, most still require substantial degree of user-interaction. In this paper, we propose a new template-driven approach that incorporates a priori knowledge about the average statistical shapes of the prostate to account for shape variability among human prostates. Unlike most deformable models that uses, as its external energy, gradient information that may contain many false edges, we use dot-pattern features found within the prostate to find the best matching contour. Our hypothesis is that distinct prostate features manifested in some regions of the ultrasound image as regular dot-like patterns can be detected using selective cells with nonlinear behavior derived from differential of Gaussian operator [8,9]. These cells react maximally to a pattern that consists of a cluster of dots regardless of their exact shapes (square or dots). In this paper we show how such intrinsic textural features consistently found within the prostate region of ultrasound images can form the basis for efficient detection of the prostate boundaries through energy minimization of a template-based, elastically-driven deformable model. A number of experiments comparing the extracted contours with manually-delineated contours are carried out to assess the efficiency of our proposed method.

2. PROSTATE SEGMENTATION

Our template driven approach is divided into three major tasks. The first task is to reduce noise and speckles that typically exist in ultrasound images and usually interfere in the segmentation process. This is accomplished via a set of pre-processing filters. The second task is to detect regular dot-like patterns that normally appear within the prostate. The energy map of this dot-pattern feature is used to drive a deformable active contour toward a global minimum. The initial contours in this model are chosen from statistical shapes that were obtained from a set of manually-outlined contours. An elastically constrained deformation ensures that the original contour shape is preserved. An iterative search is applied to find the contour that best achieves a global minimum.

2.1. Noise Removal Filtering

2.1.1. Median Filtering

Median filter is first applied to reduce impulsive noise. This non-linear filtering modifies the gray-levels of the image while preserving the original information. The center pixel of a 5x5 window is substituted with the median value of all the pixels in the window.

2.1.2. Top-Hat Transform

Top-hat transform filter is applied by morphological opening the image by a flat-top hexagon structure element with a radius of 9. Morphological operation is a well-known procedure in image processing. The opening of an image A is obtained by first eroding the image with a structure element B, after which one performs dilation on this eroded image with the same structure element. Mathematically, opening of A by B is defined as:

$$A \circ B = (A \Theta B) \oplus B \qquad (1)$$

This process removes peaks of image surfaces smaller than hexagon leaving slowly varying background. This gray-level variation is further removed by subtracting the opened image from the original image. The resulting image difference image contains little or no information in the regions of low-signal amplitude (Fig. 1).

2.2. Dot Pattern Select Cells

The dot-pattern selective method is a biologically motivated approach that is known to be effective in extracting particular class of features. This nonlinear operator is modeled with cells that are selective to dot-like patterns with regular geometric distribution. These clusters of patterns, which are the result of tissue granularity, are always found spread across most of the prostate region in an ultrasound image. The selective cells are not affected by the size, shape or orientation of these dots as long as they are equidistant from each others.

Individual dot elements within dot-patterns, which are mainly spots of varying light intensity, are first detected by the selective cells. These cells react strongly to intensity spots (intensity increments or decrements) of appropriate size. The spatial summation property of such a cell is modeled by a difference of Gaussians function (DOG) [9]:

$$DOG\,(x,y) = \frac{Ac}{\gamma^2} e^{-\frac{x^2+y^2}{2\gamma^2\sigma^2}} + A_s e^{-\frac{x^2+y^2}{2\sigma^2}} \qquad (2)$$

where the image point coordinates x and y specify the position of a light impulse (spot) in the image field. The coefficients A_c and A_s are selected in such a way that all positive values of the DOG add up to 1 and all negative values add up to -1. The parameters σ and γ describe the standard deviation and the center of the surround Gaussian functions. Figure 2 shows a 1D and 2D map of the DOG function. After a group of cells are activated by a cluster of individual dots or spots, their cumulative response are combined into one response of a subunit. The response of a population of such cells that cover uniformly the visual field as represented by the frame of the input image, and have the same form but are centered at different positions, are computed by convolving the input image *g* with the DOG function such that:

$$u(x,y) = |g * DOG\,| \qquad (3)$$

Contrast normalization is also performed by dividing the combined response by the average gray level of the image within the visual field.

$$I(x,y) = \frac{u(x,y)}{CS_{\sigma_{\max}}(x,y)+1} \tag{4}$$

Where C is a positive coefficient and $S_{\sigma_{\max}}$ is the local grey level average computed by convolving the input image with the Gaussian function with the largest standard deviation among those used. This step reduces the dependence of the strength of the response on the local contrast of the features. At this point, contiguous dot-pattern activity regions in the center cell are reduced to a single pixel. Finally, Lateral inhibition and a winner-takes-all technique are applied to suppress all responses to sub-optimal spots [9].

The spot-detector described above has been shown to be sensitive to spots of specific size in the visual field, independent of the contrast and discarding other image features such as lines and edges. The intensity of a pixel in a result image represents the response of the corresponding cell centered at that pixel. The effectiveness of the spot-detector in detecting dot-pattern features in prostate ultrasound images is illustrated in figure 3. Although isolated features can be seen scattered across the image, the majority of these spots are concentrated around the middle of the prostate. When the original unfiltered prostate image was presented to the spot-detector operator, the detected features were no longer confined to the prostate (Fig. 3, right). In this case, speckles were erroneously detected as well. This demonstrates the importance of noise-reduction to the overall process.

2.3 Deformable Template

Our energy-based approach to segmentation is achieved with an elastic deformable template [10]. This template is a 2D surface, whose initial shape reflects a priori knowledge about the prostate. Considering the elliptical shape of the prostate, the initial contour is generated experimentally from a set of elliptical curves matched to a set of manually-extracted contours. During the process of detection, the model evolves in such a way that the following energy function is minimized:

$$E_{tot} = \sum E_{\text{int}} + \sum E_{ext} + \Delta E_{ext} \tag{5}$$

$$E_{int}(v_i) = \alpha \,||\, v_i - v_{i-1} \,||^2 + \beta \,||\, v_{i-1} - 2v_i - v_{i+1} \,||^2 \tag{6}$$

$$E_{ext} = -\lambda \sum I^2(x,y) \tag{7}$$

where $I(x,y)$ is the dot-pattern image obtained from equation 4. The internal energy E_{int} will pull the contour towards a smooth curve, while the external energy E_{ext} will pull towards maximum dot-pattern energy. The gradient term ΔE_{ext} has been added to prevent the contour from being pulled toward false minima. The parameters α and β in the internal energy term describe the magnitude of elasticity and rigidity of the deformed contour, respectively. Contours with large α will not stretch or shrink easily while contours with large β will not bend easily. In order to elastically constrain the model to preserve the geometric shape of the model, we choose α and β be 0.01 and 2 respectively. The external energy term E_{ext} drives the shape model to the prostate boundaries such that the dot-pattern energy contained is maximized. The parameter γ is the weight of the external energy to the overall deformation process and was chosen experimentally to be 0.6. Five Initial shape templates $\{T_1 \ldots T_M\}$ were built from subsets of manually outlined contours $\{S_1 \ldots S_N\}$ such that:

$$T_i = \frac{M}{N} \sum_{j=i.n} S_j \qquad \textit{Where } n = 1...N/M \tag{8}$$

which represents the mean curve of every subset in $\{S_i\}$. The details of the alignment of curves (rotation, translation and scaling) for the purpose of averaging can be found in [13]. The templates $\{T_i\}$ were selected as initial contour candidates. All five contour templates were then allowed to evolve through iterative elastic deformation until the energy value in equation 5 reached a global minimum. The contour T that provided the minimal energy was finally designated as the ground-truth contour. The segmentation process requires a rough positioning of the model on the ultrasound image. Again, we use prior anatomical information of the prostate contour to obtain an approximate position and orientation of the prostate contour with respect to the ultrasound probe. Figure 4 shows an optimal contour obtained by the energy minimization algorithm superimposed on both the energy map image as well as the original prostate image.

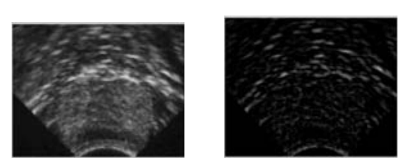

Figure 1: Original TRUS image of the prostate (left). The image after applying median filtering and morphological top-hat transform (right).

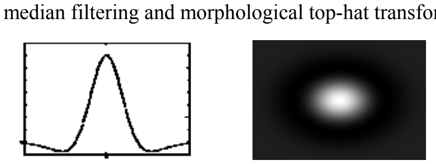

Figure 2: One-dimensional DOG profile (left). Intensity map of a two-dimensional DOG function (right).

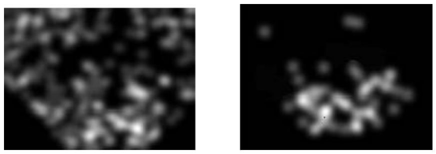

Figure 3: Result of applying dot-pattern detector to the original image in (left) and to the top-hat transformed image (right).

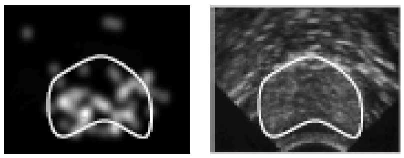

Figure 4: Deformed contour at maximum dot-pattern energy (left). Contour superimposed on original image (right).

Individual	Distance(Pixels)	Overlap Area Error %
1	17	3.2
2	11	7.2
3	18	4.6

Table 1: Comparison of the energy-based contours and manually segmented contours.

3. EXPIREMENTAL RESULTS

In this section, we evaluate our algorithm by comparing the energy-based segmentations and manual segmentations of ten ultrasound images. The original images are 8-bits pixels of size 489x382. Ten manually-segmented ultrasound images of 3 different individuals were obtained and compared with results from the proposed method. An error analysis on the overlapping area between the segmented areas using the manual and automatic segmentation method is shown in Table 1. In order to calculate the maximal shortest distance error, we find the distance to the closest point on the contour drawn by the expert and we take the maximum of the distances over the contour produced by the algorithm. The overlap area error is the overlap between the manual segmentation and automatic segmentation contours. Our algorithm has demonstrated an accuracy of at least 92%. Few factors may have influenced the accuracy of our method including the limited number of the template candidates.

4. CONCLUSION

An energy-based, template-driven segmentation scheme has been presented in this paper, for extracting prostate boundaries from TRUS images. This new proposed method relies on detection of a special class of textural elements within the prostate. The method reveals unique properties of prostate ultrasound features that may form basis for future segmentation techniques. Although the results clearly demonstrate the accuracy of our energy-minimizing approach, further validation of these dot-pattern models is needed with more prostate images of various geometric and textural features. Also, a parametric shape contour may also be more efficient in creating a larger set of templates with higher level of accuracy.

5. ACKNOWLEDGEMENT

This work was supported in part by grants from: NIH, CA90524, CA109625.

6. REFERENCES

[1] A, Zaim, R, Keck, R, S, Selman, and J, Jankun, "Three-Dimensional Ultrasound Image Matching System for Photodynamic Therapy", *Proceedings of BIOS-SPIE*, vol. 4244: pp. 327-337, 2001.

[2] J. Jankun and A. Zaim, "An image-guided robotic System for photodynamic Therapy of the Prostate," *SPIE Proceeding*, vol. 39, pp. 22-29, 1999.

[3] A. Ghanei, H. Soltanian-Zadeh, A. Ratkesicz and F. Yin, "A three-dimensional deformable model for segmentation of human prostate from ultrasound image", *Medical Physics*, vol. 28, pp. 2147–2153, 2001.

[4] N. Hu, D. Downey, A. Fenster, and H. Ladak, "Prostate surface segmentation from 3D ultrasound images", *IEEE International Symposium on Biomedical Imaging*, pp. 613–616, 2002.

[5] S.D. Pathak, V. Chalana, D.R. Haynor, "Edge-Guided Boundary Delineation in Prostate Ultrasound Images", *IEEE Trans. Med. Img*., vol. 19, pp. 1211-1219, 2000.

[6] D. Shen, Y. Zhan and C. Davatzikos, "Segmentation Prostate Boundaries from Ultrasound Images Using Statistical Shape Model", *IEEE Trans. On Med. Img*., Vol.22, pp. 539–551, 2003.

[7] R. Aarnink., A.L. Huyanen, J. "Automated prostate volume determination with ultrasonographic imaging," *Journal of Urology*, vol. 155, pp. 1038-1039, 1996.

[8] P. Kruizinga and N. Petkov, "Computational model of dot pattern selective cells" *Biological Cybernetics*, vol. 83, no. 4, pp. 313–325, 2000.

[9] N. Petkov and W. Visser, "Modifications of center-surround, spot detection and dot-pattern detection selective operators." Technical Reports 2005-9-01, *Institute of Mathematics and Computing Science*, 20 January 2005.

[10] M, Kass, A. Witkin, and D. Terzopoulos "Snakes: Active contour models" *IJCV*, vol.1(4), pp. 321-331, 1987.

[11] A. Pitiot, A. Toga, and P. Thompson, "Adaptive elastic segmentation of brain MRI via shape-model-guided evolutionary programming" *IEEE Transaction Medical Imaging*, vol. 21, no. 8, pp. 910-923, 2002.